

- ¹ Institute of High Energy Physics, Beijing 100049, People's Republic of China
- ² Beihang University, Beijing 100191, People's Republic of China
- ³ Beijing Institute of Petrochemical Technology, Beijing 102617, People's Republic of China
- ⁴ Bochum Ruhr-University, D-44780 Bochum, Germany
- ⁵ Carnegie Mellon University, Pittsburgh, Pennsylvania 15213, USA
- ⁶ Central China Normal University, Wuhan 430079, People's Republic of China
- ⁷ Central South University, Changsha 410083, People's Republic of China
- ⁸ China Center of Advanced Science and Technology, Beijing 100190, People's Republic of China
- ⁹ COMSATS University Islamabad, Lahore Campus, Defence Road, Off Raiwind Road, 54000 Lahore, Pakistan
- ¹⁰ Fudan University, Shanghai 200433, People's Republic of China
- ¹¹ G.I. Budker Institute of Nuclear Physics SB RAS (BINP), Novosibirsk 630090, Russia
- ¹² GSI Helmholtzcentre for Heavy Ion Research GmbH, D-64291 Darmstadt, Germany
- ¹³ Guangxi Normal University, Guilin 541004, People's Republic of China
- ¹⁴ Guangxi University, Nanning 530004, People's Republic of China
- ¹⁵ Hangzhou Normal University, Hangzhou 310036, People's Republic of China
- ¹⁶ Hebei University, Baoding 071002, People's Republic of China
- ¹⁷ Helmholtz Institute Mainz, Staudinger Weg 18, D-55099 Mainz, Germany
- ¹⁸ Henan Normal University, Xinxiang 453007, People's Republic of China
- ¹⁹ Henan University of Science and Technology, Luoyang 471003, People's Republic of China
- ²⁰ Henan University of Technology, Zhengzhou 450001, People's Republic of China
- ²¹ Huangshan College, Huangshan 245000, People's Republic of China
- ²² Hunan Normal University, Changsha 410081, People's Republic of China
- ²³ Hunan University, Changsha 410082, People's Republic of China
- ²⁴ Indian Institute of Technology Madras, Chennai 600036, India
- ²⁵ Indiana University, Bloomington, Indiana 47405, USA
- ²⁶ INFN Laboratori Nazionali di Frascati, (A)INFN Laboratori Nazionali di Frascati, I-00044, Frascati, Italy; (B)INFN Sezione di Perugia, I-06100, Perugia, Italy; (C)University of Perugia, I-06100, Perugia, Italy
- ²⁷ INFN Sezione di Ferrara, (A)INFN Sezione di Ferrara, I-44122, Ferrara, Italy; (B)University of Ferrara, I-44122, Ferrara, Italy
- ²⁸ Institute of Modern Physics, Lanzhou 730000, People's Republic of China
- ²⁹ Institute of Physics and Technology, Peace Avenue 54B, Ulaanbaatar 13330, Mongolia
- ³⁰ Jilin University, Changchun 130012, People's Republic of China
- ³¹ Johannes Gutenberg University of Mainz, Johann-Joachim-Becher-Weg 45, D-55099 Mainz, Germany
- ³² Joint Institute for Nuclear Research, 141980 Dubna, Moscow Region, Russia
- ³³ Justus-Liebig-Universitaet Giessen, II. Physikalisches Institut, Heinrich-Buff-Ring 16, D-35392 Giessen, Germany
- ³⁴ Lanzhou University, Lanzhou 730000, People's Republic of China
- ³⁵ Liaoning Normal University, Dalian 116029, People's Republic of China
- ³⁶ Liaoning University, Shenyang 110036, People's Republic of China
- ³⁷ Nanjing Normal University, Nanjing 210023, People's Republic of China
- ³⁸ Nanjing University, Nanjing 210093, People's Republic of China
- ³⁹ Nankai University, Tianjin 300071, People's Republic of China
- ⁴⁰ National Centre for Nuclear Research, Warsaw 02-093, Poland
- ⁴¹ North China Electric Power University, Beijing 102206, People's Republic of China
- ⁴² Peking University, Beijing 100871, People's Republic of China
- ⁴³ Qufu Normal University, Qufu 273165, People's Republic of China
- ⁴⁴ Shandong Normal University, Jinan 250014, People's Republic of China
- ⁴⁵ Shandong University, Jinan 250100, People's Republic of China
- ⁴⁶ Shanghai Jiao Tong University, Shanghai 200240, People's Republic of China
- ⁴⁷ Shanxi Normal University, Linfen 041004, People's Republic of China
- ⁴⁸ Shanxi University, Taiyuan 030006, People's Republic of China
- ⁴⁹ Sichuan University, Chengdu 610064, People's Republic of China
- ⁵⁰ Soochow University, Suzhou 215006, People's Republic of China
- ⁵¹ South China Normal University, Guangzhou 510006, People's Republic of China
- ⁵² Southeast University, Nanjing 211100, People's Republic of China
- ⁵³ State Key Laboratory of Particle Detection and Electronics, Beijing 100049, Hefei 230026, People's Republic of China
- ⁵⁴ Sun Yat-Sen University, Guangzhou 510275, People's Republic of China
- ⁵⁵ Suranaree University of Technology, University Avenue 111, Nakhon Ratchasima 30000, Thailand
- ⁵⁶ Tsinghua University, Beijing 100084, People's Republic of China
- ⁵⁷ Turkish Accelerator Center Particle Factory Group, (A)Istinye University, 34010, Istanbul, Turkey; (B)Near East University, Nicosia, North Cyprus, Mersin 10, Turkey
- ⁵⁸ University of Chinese Academy of Sciences, Beijing 100049, People's Republic of China
- ⁵⁹ University of Groningen, NL-9747 AA Groningen, Netherlands
- ⁶⁰ University of Hawaii, Honolulu, Hawaii 96822, USA
- ⁶¹ University of Jinan, Jinan 250022, People's Republic of China
- ⁶² University of Manchester, Oxford Road, Manchester, M13 9PL, United Kingdom

⁶³ University of Muenster, Wilhelm-Klemm-Strasse 9, 48149 Muenster, Germany

⁶⁴ University of Oxford, Keble Road, Oxford, OX13RH, United Kingdom

⁶⁵ University of Science and Technology Liaoning, Anshan 114051, People's Republic of China

⁶⁶ University of Science and Technology of China, Hefei 230026, People's Republic of China

⁶⁷ University of South China, Hengyang 421001, People's Republic of China

⁶⁸ University of the Punjab, Lahore-54590, Pakistan

⁶⁹ University of Turin and INFN, (A)University of Turin, I-10125, Turin, Italy; (B)University of Eastern Piedmont, I-15121, Alessandria, Italy; (C)INFN, I-10125, Turin, Italy

⁷⁰ Uppsala University, Box 516, SE-75120 Uppsala, Sweden

⁷¹ Wuhan University, Wuhan 430072, People's Republic of China

⁷² Xinyang Normal University, Xinyang 464000, People's Republic of China

⁷³ Yunnan University, Kunming 650500, People's Republic of China

⁷⁴ Zhejiang University, Hangzhou 310027, People's Republic of China

⁷⁵ Zhengzhou University, Zhengzhou 450001, People's Republic of China

⁷⁶ China University of Geosciences, Wuhan 430074, People's Republic of China

^a Also at the Moscow Institute of Physics and Technology, Moscow 141700, Russia

^b Also at the Novosibirsk State University, Novosibirsk, 630090, Russia

^c Also at the NRC "Kurchatov Institute", PNPI, 188300, Gatchina, Russia

^d Also at Goethe University Frankfurt, 60323 Frankfurt am Main, Germany

^e Also at Key Laboratory for Particle Physics, Astrophysics and Cosmology, Ministry of Education; Shanghai Key Laboratory for Particle Physics and Cosmology; Institute of Nuclear and Particle Physics, Shanghai 200240, People's Republic of China

^f Also at Key Laboratory of Nuclear Physics and Ion-beam Application (MOE) and Institute of Modern Physics, Fudan University, Shanghai 200443, People's Republic of China

^g Also at State Key Laboratory of Nuclear Physics and Technology, Peking University, Beijing 100871, People's Republic of China

^h Also at School of Physics and Electronics, Hunan University, Changsha 410082, China

ⁱ Also at Guangdong Provincial Key Laboratory of Nuclear Science, Institute of Quantum Matter, South China Normal University, Guangzhou 510006, China

^j Also at Frontiers Science Center for Rare Isotopes, Lanzhou University, Lanzhou 730000, People's Republic of China

^k Also at Lanzhou Center for Theoretical Physics, Lanzhou University, Lanzhou 730000, People's Republic of China

^l Also at the Department of Mathematical Sciences, IBA, Karachi, Pakistan

(Dated: February 26, 2023)

Using a sample of 4.3×10^5 $\eta' \rightarrow \eta\pi^0\pi^0$ events selected from the ten billion J/ψ event dataset collected with the BESIII detector, we study the decay $\eta' \rightarrow \eta\pi^0\pi^0$ within the framework of nonrelativistic effective field theory. Evidence for a structure at $\pi^+\pi^-$ mass threshold is observed in the invariant mass spectrum of $\pi^0\pi^0$ with a statistical significance of around 3.5σ , which is consistent with the cusp effect as predicted by the nonrelativistic effective field theory. After introducing the amplitude for describing the cusp effect, the $\pi\pi$ scattering length combination $a_0 - a_2$ is determined to be $0.226 \pm 0.060_{\text{stat}} \pm 0.013_{\text{sys}}$, which is in good agreement with theoretical calculation of 0.2644 ± 0.0051 .

Experimental studies of light meson decays are important guides to our understanding of how QCD works in the non-perturbative regime. In this context, the $\pi\pi$ and πK interactions at low energies have been the subject of investigations for a few decades. In $\pi\pi$ interaction, one of the prominent features is the loop contribution to the $\pi\pi$ scattering: the S -wave charge-exchange rescattering $\pi^+\pi^- \rightarrow \pi^0\pi^0$ (as shown in Fig. 1) causes a prominent cusp at the center of mass energy corresponding to the summed mass of two charged pions. The cusp effect can shed light on the fundamental properties of QCD at low energies, by determining the strength of the S -wave $\pi\pi$ interaction [1–6]. Six decades ago this effect was predicted to be seen in $K^+ \rightarrow \pi^0\pi^0\pi^+$ [7], and it was finally observed in 2006 [8] by the NA48/2 experiment and studied further [9]. These results inspired theoretical predictions for the cusp in other decays, such as $K_L \rightarrow 3\pi^0$ [3, 5, 10] and $\eta \rightarrow 3\pi^0$ [11, 12], which were experimentally investigated: it was observed in the decay of $K_L \rightarrow 3\pi^0$ by KTeV [13], while no clear evidence was seen in $\eta \rightarrow 3\pi^0$ decay [14–17].

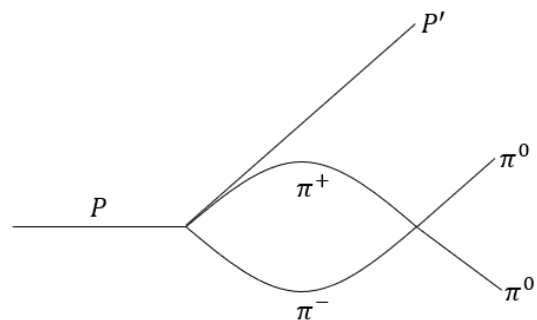


FIG. 1. One-loop contribution in $P \rightarrow P'\pi^0\pi^0$ decay, where P and P' denote pseudoscalar particles in initial and final states, respectively. Different behaviors below and above the charged pion mass threshold cause the cusp effect.

Another process where the cusp effect is expected to have a sizable contribution is the hadronic decay $\eta' \rightarrow \eta\pi^0\pi^0$ [18];

this has been experimentally investigated by BESIII [19], with 5.6×10^4 $\eta' \rightarrow \eta\pi^0\pi^0$ events, and no evidence was seen, while the A2 experiment [20] accumulated about 1.24×10^5 $\eta' \rightarrow \eta\pi^0\pi^0$ decays and reported a deviation with a significance of about 2.5σ and it is also studied in chiral perturbation theory [21]. Therefore, it is essential to further investigate this decay with higher precision.

The recently available data of ten billion J/ψ events [22] at BESIII imply an increased data sample of η' decays by nearly an order of magnitude, offering a unique opportunity for further investigations of the cusp effect. In this Letter, we present the first evidence of the cusp effect in $\eta' \rightarrow \eta\pi^0\pi^0$ and the corresponding measurement of the $\pi\pi$ scattering length based on the nonrelativistic effective field theory (NREFT) [18].

The BESIII detector [23, 24] records symmetric e^+e^- collisions provided by the BEPCII storage ring [25]. The cylindrical core of the BESIII detector covers 93% of the full solid angle and consists of a helium-based multilayer drift chamber (MDC), a plastic scintillator time-of-flight (TOF) system, and a CsI(Tl) electromagnetic calorimeter (EMC), which are all enclosed in a superconducting solenoidal magnet providing a 1.0 T (0.9 T in 2012) magnetic field. The end cap TOF system was upgraded in 2015 using multigap resistive plate chamber technology [26–28].

To reconstruct events of $J/\psi \rightarrow \gamma\eta'$ with $\eta' \rightarrow \eta\pi^0\pi^0$, the π^0 and η are selected by $\pi^0/\eta \rightarrow 2\gamma$ process. The charged tracks are reconstructed from hits in the MDC. The polar angle with respect to the MDC symmetry axis should be in the range $|\cos\theta| < 0.93$. The distance away from the interaction point should be less than 10.0 cm in the beam direction and 1.0 cm in the radial direction. The photon candidates are reconstructed using clusters of energy deposited in the EMC. The energy deposited in the nearby TOF system is included in EMC measurements to improve the reconstruction efficiency and the energy resolution. Photon candidates are required to have a deposited energy larger than 25 MeV in the barrel region ($|\cos\theta| < 0.80$) and 50 MeV in the end cap regions ($0.86 < |\cos\theta| < 0.92$). A requirement on the EMC cluster timing with respect to the most energetic photon, $-500 < T < 500$ ns, is used to suppress electronic noise and energy deposits unrelated to the event. The events with at least seven photon candidates and no charged tracks are kept for further analysis.

For each candidate event, the photon with the maximum energy is assumed to be the radiative photon originating from the decay of J/ψ , while the remaining photons are used to reconstruct π^0/η candidates. A one-constraint (1C) kinematic fit is performed by constraining the invariant mass of photon pairs to the π^0 or η mass, and the χ^2 for this fit is required to be less than 25. Since the π^0 decays into two photons isotropically in its rest frame, the angle of one photon in the π^0 rest frame with respect to the π^0 momentum direction is required to satisfy $|\cos\theta_{\pi^0}| < 0.95$. Afterward, an eight-constraint (8C) kinematic fit is performed for the $\gamma\eta\pi^0\pi^0$ combinations, requiring energy-momentum conservation and constraining the invariant masses of the three photon pairs to the nominal π^0/η

masses and of the $\eta\pi^0\pi^0$ combinations to the η' mass. If more than one $\gamma\eta\pi^0\pi^0$ combination is found, only the one with the least χ_{8C}^2 is retained. After the requirement of $\chi_{8C}^2 < 100$, 432295 candidate events are accepted for further analysis; the corresponding Dalitz plot is shown in Fig. 2.

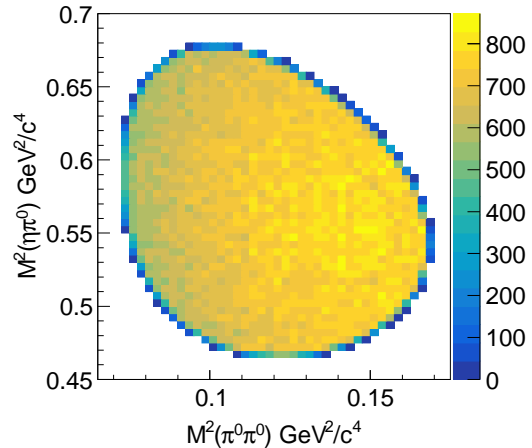


FIG. 2. Dalitz plot of $\eta' \rightarrow \eta\pi^0\pi^0$.

To investigate the background contamination, a 6C kinematic fit, instead of the 8C fit, is performed on candidate events, in which the constraints on the masses of η and η' are removed. Figure 3 shows the $\eta\pi^0\pi^0$ invariant mass distribution of the data sample, after requiring $\chi_{6C}^2 < 100$ and η mass window cut $|M(\gamma\gamma) - M_\eta| < 30$ MeV/ c^2 on the unconstrained photon pair, a clear η' peak is observed. In addition, a ten billion J/ψ inclusive decay Monte Carlo (MC) sample generated with LUNDCHARM [29, 30] is used to check possible background sources; the surviving events mainly consist of the peaking background $\eta' \rightarrow 3\pi^0$ decay channel and the flat contribution from $J/\psi \rightarrow \omega\eta$, with $\omega \rightarrow \gamma\pi^0$ and $\eta \rightarrow 3\pi^0$. The background contamination rate is estimated about 0.82%, and its shape on $\pi^0\pi^0$ and $\eta\pi^0$ mass spectrum is smooth; therefore, it is neglected in the further analysis.

Using an unbinned maximum likelihood method, we fit the Dalitz plot of $M^2(\pi^0\pi^0)$ versus $M^2(\eta\pi^0)$ within the framework of NREFT. (More details are given in the Supplemental Material [31].) The resolution effect and detection efficiency are studied by MC simulation and taken into account in the fit.

In the simplest case (fit I), only the tree level contribution is included in which the final state interaction effect is ignored. In this case, the amplitude is the same as the general parametrization used in Ref. [19]. The projections of the fit result to the Dalitz coordinates X and Y are shown in Figs. 4(a) and 4(b), and they indicate a good description of data. The fitted parameter values, shown in Table I, are consistent with the previous BESIII measurement and the statistical uncertainties are about one third of the previous results [19]. In Figs. 4(c) and 4(d) the comparisons between data and the fit projections of the $\eta\pi^0$ and $\pi^0\pi^0$ invariant mass distributions divided by

TABLE I. Experimental values of the matrix element parameters for $\eta' \rightarrow \eta\pi^0\pi^0$.

| Parameters | Fit I | Fit II | Fit III | Fit IV |
|--------------------------|------------------------------|--------------------|--------------------|------------------------------|
| a | $-0.075 \pm 0.003 \pm 0.001$ | -0.207 ± 0.013 | -0.143 ± 0.010 | $-0.077 \pm 0.003 \pm 0.001$ |
| b | $-0.073 \pm 0.005 \pm 0.001$ | -0.051 ± 0.014 | -0.038 ± 0.006 | $-0.066 \pm 0.006 \pm 0.001$ |
| d | $-0.066 \pm 0.003 \pm 0.001$ | -0.068 ± 0.004 | -0.067 ± 0.003 | $-0.068 \pm 0.004 \pm 0.001$ |
| $a_0 - a_2$ | - | 0.174 ± 0.066 | 0.225 ± 0.062 | $0.226 \pm 0.060 \pm 0.013$ |
| a_0 | - | 0.497 ± 0.094 | - | - |
| a_2 | - | 0.322 ± 0.129 | - | - |
| Statistical significance | - | 3.4σ | 3.7σ | 3.6σ |

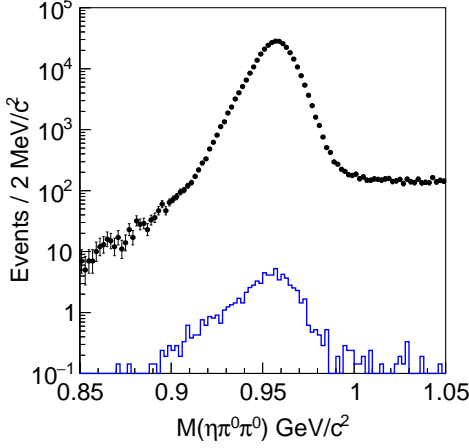


FIG. 3. The $\eta\pi^0\pi^0$ invariant mass distribution after 6C kinematic fit without the η and η' mass constraints. The dots with error bars are experimental data, and the blue histogram is the $\eta' \rightarrow 3\pi^0$ peaking background from MC sample.

the phase space are presented. The discrepancy between data and fit result below the charged pion mass threshold corresponds to the cusp effect. Therefore, we perform alternative fits by including the loop contributions within the framework of NREFT to evaluate this effect, and fit I is taken as the baseline for the further loop level fits.

At the loop level amplitude, only $\pi\pi$ scattering is considered while $\eta\pi$ scattering is ignored; the S -wave $\pi\pi$ scattering lengths a_0 and a_2 are included in the loop level amplitude by matching between NREFT amplitude and partial wave decomposition,

$$\begin{aligned}
 C_{00} &= \frac{16\pi}{3}(a_0 + 2a_2)(1 - \xi), \\
 C_x &= \frac{16\pi}{3}(a_2 - a_0)\left(1 + \frac{\xi}{3}\right), \\
 C_{+-} &= \frac{8\pi}{3}(2a_0 + a_2)(1 + \xi), \\
 \xi &= \frac{M_{\pi^\pm}^2 - M_{\pi^0}^2}{M_{\pi^\pm}^2}.
 \end{aligned} \tag{1}$$

where C_x denotes the coupling coefficient of the cusp term $\pi^+\pi^- \rightarrow \pi^0\pi^0$, and C_{00} and C_{+-} are the coupling coefficients

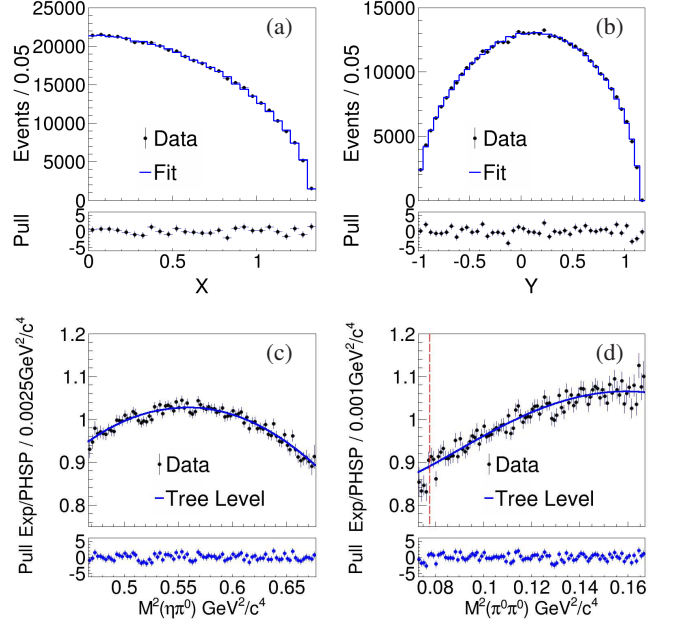


FIG. 4. The fit result of fit I. The projections to X and Y are shown in (a) and (b), and the mass spectrums of $M^2(\eta\pi^0)$ and $M^2(\pi^0\pi^0)$ divided by phase space are shown in (c) and (d). The black dots with error bars are from data and the blue line is the fit result of the tree level amplitude. The red dashed line indicates the charged pion mass threshold.

of noncusp terms $\pi^0\pi^0 \rightarrow \pi^0\pi^0$ and $\pi^+\pi^- \rightarrow \pi^+\pi^-$, which are defined in Ref. [18].

The distribution of $M^2(\pi^0\pi^0)$ is determined by the whole amplitude and all five parameters a , b , d , a_0 , and a_2 , while the distribution of $M^2(\eta\pi^0)$ is mainly determined by parameter d , where a , b and d are coefficients in tree level amplitude.

To verify the prediction of NREFT and evaluate the scattering length combination $a_0 - a_2$, we perform many unbinned maximum likelihood fits in different cases after including the contributions from the amplitudes at one- and two-loop levels.

In the case when all the parameters are free (fit II), the fit quality is improved, and we obtain a statistical significance of 3.4σ compared to fit I. In Fig. 5, the comparison between the fit and data for the projections in different variables, as well as the pull distributions, shows that the fit provides a good description, in particular, for the region below the charged

pion mass threshold. However, the correlation between the four parameters a , b , a_0 , and a_2 is very large, as shown in Eq. (2). This strong correlation between a , b , a_0 , and a_2 may be caused by the loop level amplitude contribution to noncusp terms. The scattering length combination is calculated to be $a_0 - a_2 = 0.174 \pm 0.066$,

$$\left(\begin{array}{c|ccc} & b & d & a_0 - a_2 \\ \hline a & 0.831 & 0.189 & -0.966 \\ b & & 0.348 & -0.918 \\ d & & & -0.257 \\ a_0 & & & 0.872 \end{array} \right) \quad (2)$$

To reduce the correlations between parameters, we also made an attempt (fit III) by fixing $a_0 + 2a_2 = 0.1312$ according to the theoretical values $a_0 = 0.220 \pm 0.005$ and $a_2 = -0.0444 \pm 0.0010$ [18] and setting $a_0 - a_2$ as a free parameter, since only C_x contributes to the cusp effect. The fit result presented in Fig. 5 shows a good agreement with data, also in the region below the charged pion mass threshold. The fitted parameter values are summarized in Table I, and the corresponding correlations are shown in Eq. (3); the obtained value of $a_0 - a_2 = 0.225 \pm 0.062$ is in agreement with the theoretical value 0.2644 ± 0.0051 [18]. We also test by changing the value of $a_0 + 2a_2$ or fixing both $a_0 + 2a_2$ and $2a_0 + a_2$ to theoretical values, the fit results are consistent with the result of fit III, and $a_0 - a_2$ is not sensitive to fixed value,

$$\left(\begin{array}{c|ccc} & b & d & a_0 - a_2 \\ \hline a & -0.560 & -0.046 & -0.955 \\ b & & 0.249 & 0.457 \\ d & & & -0.032 \end{array} \right) \quad (3)$$

Comparing to the tree level amplitude, the loop contributions with C_{00} and C_{+-} are expected to be small. Additionally, we performed an alternative fit (fit IV) by ignoring non-cusp terms with C_{00} and C_{+-} and only introducing the decay amplitude with C_x for the description of the cusp effect. In this case, the fitted values of different parameters, summarized in Table I, are in agreement with those of fit I, the correlations shown in Eq. (4) are reduced and the statistical significance of the cusp effect is 3.6σ , while the scattering length combination $a_0 - a_2 = 0.226 \pm 0.060$ is consistent with that in Ref. [18]. In addition, we found that the log-likelihood value of fit IV is very close to those of fit II fit III, which implies that the introduction of the loop contributions with C_{00} and C_{+-} has little impact on the improvement of the fit quality and the cusp effect, but significantly increases the correlations between the different parameters. Therefore, in this analysis, it is reasonable to ignore these loop contributions in fitting

data,

$$\left(\begin{array}{c|ccc} & b & d & a_0 - a_2 \\ \hline a & -0.363 & -0.253 & 0.126 \\ b & & 0.257 & 0.237 \\ d & & & -0.107 \end{array} \right) \quad (4)$$

The systematic uncertainties for the Dalitz plots analysis are listed in Table II. We calculate the total systematic uncertainty by assuming that all the contributions are independent and adding them in quadrature.

The photon detection efficiency is studied with the control sample of $J/\psi \rightarrow \rho^0 \pi^0$ events. To evaluate the impact from the slight discrepancy between data and MC simulation, we perform a correction on the photon detection and the change of the fit results is considered as the systematic uncertainty.

To estimate the uncertainties from the 1C kinematic fit for π^0 and η , we selected as control samples $J/\psi \rightarrow \pi^+ \pi^- \pi^0$ and $J/\psi \rightarrow \gamma \eta'$ with $\eta' \rightarrow \eta \pi^+ \pi^-$, without kinematic fit. After taking into account the discrepancy between data and MC simulation, repeating the fit with the weighted events leads to changes of the parameter values, which are assigned as the systematic uncertainties.

To check if the photon miscombinations can effect the fitted parameters, we generate a MC sample based on NREFT amplitude and tag miscombination events by matching the truth and the reconstructed value of photon momentum. Two fits are performed to the sample with and without miscombination events, and the change of the results is taken as the systematic uncertainty.

To evaluate the uncertainty associated with the efficiency parametrization, we change the Dalitz plot variables to $M^2(\eta\pi)$ and $\cos\theta$, where θ is the angle between the directions of the two π s in the rest frame of $\eta\pi$. We repeat the fit based on the newly defined Dalitz plot variables, and the change of the resulting parameters with respect to the nominal results is assigned as the systematic uncertainty.

The uncertainty of the 8C kinematic fit mainly comes from the inconsistency of the photon resolution between data and MC simulation. We adjust the energy resolution in the reconstructed photon error matrix to ensure that the MC simulation provides a good description of data. Afterward, an alternative fit is performed and the change of the fitted parameters with respect to the nominal result is taken as the systematic uncertainty.

To estimate the uncertainty from resolution effect, we vary the resolution by $\pm 10\%$ and perform alternative fits. The maximum change with respect to the nominal result is taken as the systematic uncertainty.

In summary, using ten billion J/ψ events collected with the BESIII detector, we select a $\eta' \rightarrow \eta \pi^0 \pi^0$ sample 8 times larger than that previously analyzed by BESIII, and perform a Dalitz plot analysis within the framework of nonrelativistic effective field theory. The fit with tree level amplitude shows a discrepancy below the charged pion mass threshold, which implies the existence of the cusp effect. To describe the data

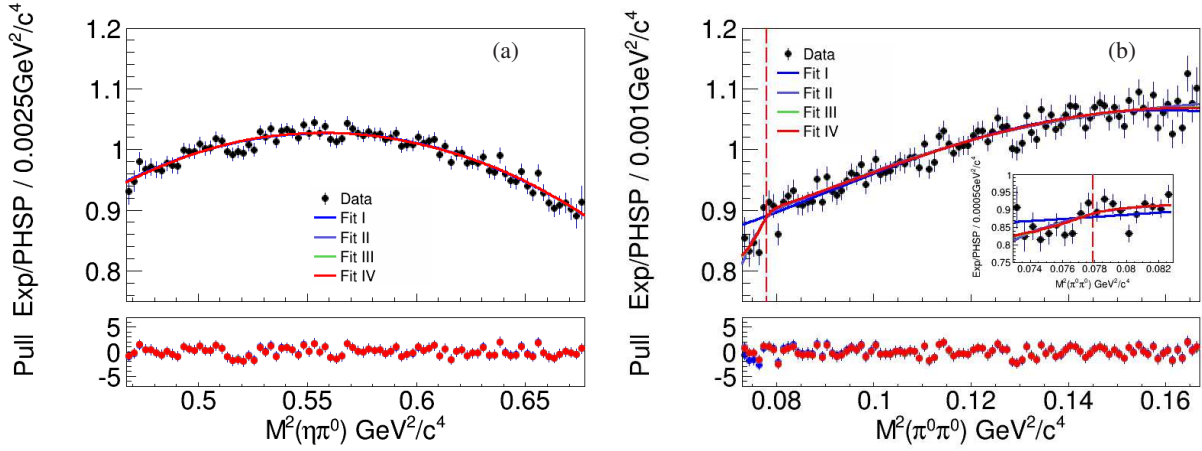


FIG. 5. The fit result projections divided by phase space of different models to variable (a) $M^2(\eta\pi^0)$ and (b) $M^2(\pi^0\pi^0)$. The black dots with error bars are from data. The solid lines are fit results from the corresponding models. The red dashed line indicates the charged pion mass threshold. The cusp region is also shown in the inset.

TABLE II. Summary of the systematic uncertainty sources and their corresponding contributions (%).

| Parametrization | Fit I | | | Fit IV | | | $a_0 - a_2$ |
|--------------------------|-------|-----|-----|--------|-----|-----|-------------|
| | a | b | d | a | b | d | |
| Source | a | b | d | a | b | d | $a_0 - a_2$ |
| Photon detection | 0.7 | 0.4 | 1.0 | 0.6 | 0.4 | 0.9 | 1.8 |
| η 1C kinematic fit | 0.1 | 0.6 | 0.0 | 0.1 | 0.7 | 0.0 | 0.2 |
| π^0 1C kinematic fit | 0.1 | 0.2 | 1.0 | 0.1 | 0.2 | 0.9 | 0.3 |
| Photon miscombination | 0.0 | 0.2 | 1.1 | 0.0 | 0.2 | 1.1 | 1.6 |
| Efficiency presentation | 0.7 | 1.0 | 0.4 | 0.7 | 0.9 | 0.4 | 1.9 |
| Kinematic fit | 0.5 | 1.3 | 0.7 | 0.4 | 0.9 | 0.8 | 4.2 |
| Resolution | 0.0 | 0.0 | 0.0 | 0.1 | 0.3 | 0.0 | 2.0 |
| Total | 1.1 | 1.8 | 2.0 | 1.0 | 1.6 | 1.9 | 5.6 |

in this region, the contributions at one- and two-loop level are introduced in the decay amplitude. We perform alternative analyses by taking into account the cusp effect and the results are summarized in Table I. For each case, the amplitude provides a good description of the structure around the charged pion mass threshold and the statistical significance is found to be around 3.5σ . The scattering length combination $a_0 - a_2$ is measured to be $0.226 \pm 0.060 \pm 0.013$, which is in good agreement with the theoretical value of 0.2644 ± 0.0051 [18] within the uncertainties. The observation of the evidence of the cusp effect in $\eta' \rightarrow \eta\pi^0\pi^0$ decay demonstrates the excellent potential to investigate the underlying dynamics of light mesons at the BESIII experiment. The prospects [32] for the precise measurements are very promising at the planned Super Tau-Charm Factories [33, 34].

The BESIII Collaboration thanks the staff of BEPCII and the IHEP computing center for their strong support. This work is supported in part by National Key R&D Program of China under Contracts No. 2020YFA0406300, No. 2020YFA0406400; National Natural Science Foundation of China (NSFC) under Contracts No. 11635010, No. 11735014, No. 11835012, No. 11935015, No. 11935016,

No. 11935018, No. 11961141012, No. 12005195, No. 12022510, No. 12025502, No. 12035009, No. 12035013, No. 12192260, No. 12192261, No. 12192262, No. 12192263, No. 12192264, No. 12192265, No. 12225509; the Chinese Academy of Sciences (CAS) Large-Scale Scientific Facility Program; Joint Large-Scale Scientific Facility Funds of the NSFC and CAS under Contract No. U1832207; CAS Key Research Program of Frontier Sciences under Contract No. QYZDJ-SSW-SLH040; 100 Talents Program of CAS; IN-PAC and Shanghai Key Laboratory for Particle Physics and Cosmology; ERC under Contract No. 758462; European Union's Horizon 2020 research and innovation program under Marie Skłodowska-Curie Grant Agreement under Contract No. 894790; German Research Foundation DFG under Contracts No. 443159800, Collaborative Research Center CRC 1044, GRK 2149; Istituto Nazionale di Fisica Nucleare, Italy; Ministry of Development of Turkey under Contract No. DPT2006K-120470; National Science and Technology fund; STFC (United Kingdom); The Royal Society, UK under Contracts No. DH140054, No. DH160214; The Swedish Research Council; U. S. Department of Energy under Award No. DE-FG02-05ER41374.

Supplemental Material: A Brief Description of NREFT amplitude of $\eta' \rightarrow \eta\pi^0\pi^0$ Decay

This supplemental material is based on Ref. [18]. In the $\eta' \rightarrow \eta\pi^0\pi^0$ decay

$$\eta'(P_{\eta'}) \rightarrow \pi^0(p_1)\pi^0(p_2)\eta(p_3), \quad (5)$$

the kinematical variables s_i are defined as $s_i = (P_{\eta'} - p_i)^2$, $i = 1, 2, 3$, and $s_1 + s_2 + s_3 = M_{\eta'}^2 + M_{\eta}^2 + 2M_{\pi^0}^2$. The Dalitz plot distribution of this decay can also be described by kinematical variables X and Y

$$\begin{aligned} X &= \frac{\sqrt{3}|s_1 - s_2|}{2M_{\eta'}Q_{\eta'}} = \frac{\sqrt{3}|T_{\pi_1^0} - T_{\pi_2^0}|}{Q_{\eta'}}, \\ Y &= \frac{(M_{\eta} + 2M_{\pi^0})[(M_{\eta'} - M_{\eta})^2 - s_3]}{2M_{\eta'}M_{\pi^0}Q_{\eta'}} - 1 \\ &= \frac{(M_{\eta} + 2M_{\pi^0})T_{\eta}}{M_{\pi^0}Q_{\eta'}} - 1, \end{aligned} \quad (6)$$

where T_i denote kinetic energy of mesons in the rest frame of η' , and $Q_{\eta'} = M_{\eta'} - M_{\eta} - 2M_{\pi^0}$. The Dalitz plot distribution can be expanded by X and Y around the center of the Dalitz plot

$$|\mathcal{M}(X, Y)|^2 = |\mathcal{N}|^2(1 + aY + bY^2 + cX + dX^2 + \dots), \quad (7)$$

which is known as general parameterization. Here \mathcal{N} is a normalization factor and parameter c is fixed at 0 since two π^0 s are identical bosons. The general parameterization can be also expressed as

$$\mathcal{M}(X, Y) = \mathcal{N}\left\{1 + \frac{a}{2}Y + \frac{1}{2}\left(b - \frac{a^2}{4}\right)Y^2 + \frac{d}{2}X^2 + \dots\right\}. \quad (8)$$

The NREFT amplitude of $\eta' \rightarrow \eta\pi\pi$ can be decomposed to

$$\begin{aligned} \mathcal{M}_{\eta' \rightarrow \eta\pi^0\pi^0} &= \mathcal{M}_N^{tree} + \mathcal{M}_N^{one-loop} + \mathcal{M}_N^{two-loop} + \dots, \\ \mathcal{M}_{\eta' \rightarrow \eta\pi^+\pi^-} &= \mathcal{M}_C^{tree} + \mathcal{M}_C^{one-loop} + \mathcal{M}_C^{two-loop} + \dots \end{aligned} \quad (9)$$

The tree level amplitudes are

$$\begin{aligned} \mathcal{M}_N^{tree}(s_1, s_2, s_3) &= \sum_{i=0}^2 G_i X_3^i + G_3(X_1 - X_2)^2, \\ \mathcal{M}_C^{tree}(s_1, s_2, s_3) &= \sum_{i=0}^2 H_i X_3^i + H_3(X_1 - X_2)^2, \end{aligned} \quad (10)$$

where $X_k = p_k^0 - M_{\eta}$, $k = 1, 2, 3$, p_i^0 is the energy of particle i in the η' rest frame, and parameters G_i are the low-energy coupling coefficients of $\eta' \rightarrow \eta\pi^0\pi^0$ decay and H_i for $\eta' \rightarrow \eta\pi^+\pi^-$ decay. The charged decay mode is introduced for the further description of loop level amplitude and we assume $H_i = -G_i$ according to the isospin limit [18–20]. G_i

can be evaluated by matching to the general parameterization

$$\begin{aligned} G_0 &= \mathcal{N}\left\{1 - \frac{a}{2} + \frac{1}{2}\left(b - \frac{a^2}{4}\right)\right\}, \\ G_1 &= \mathcal{N}\left\{\frac{a}{2} - \left(b - \frac{a^2}{4}\right)\right\} \frac{M_{\eta} + 2M_{\pi^0}}{M_{\pi^0}Q_{\eta'}}, \\ G_2 &= \mathcal{N}\left(b - \frac{a^2}{4}\right) \frac{(M_{\eta} + 2M_{\pi^0})^2}{2M_{\pi^0}^2Q_{\eta'}^2}, \\ G_3 &= \mathcal{N} \frac{3d}{2Q_{\eta'}^2}. \end{aligned} \quad (11)$$

The loop level amplitude of $\eta' \rightarrow \eta\pi^0\pi^0$ decay are

$$\begin{aligned} \mathcal{M}_N^{one-loop}(s_1, s_2, s_3) &= \mathcal{B}_{N1}(s_3)J_{+-}(s_3) \\ &\quad + \mathcal{B}_{N2}(s_3)J_{00}(s_3), \\ \mathcal{M}_N^{two-loop}(s_1, s_2, s_3) &= C_{00}(s_3)\mathcal{B}_{N2}(s_3)J_{00}^2(s_3) \\ &\quad + C_{00}(s_3)\mathcal{B}_{N1}(s_3)J_{00}(s_3)J_{+-}(s_3) \\ &\quad + 2C_x(s_3)\mathcal{B}_{C2}(s_3)J_{00}(s_3)J_{+-}(s_3) \\ &\quad + 2C_x(s_3)\mathcal{B}_{C1}(s_3)J_{+-}^2(s_3), \end{aligned} \quad (12)$$

with one-loop function

$$\begin{aligned} J_{ab} &= \frac{iq_{ab}(s_k)}{8\pi\sqrt{s_k}}, \\ q_{ab}^2(s) &= \frac{\lambda(s, M_a^2, M_b^2)}{4s}, \\ \lambda(a, b, c) &= a^2 + b^2 + c^2 - 2(ab + ac + bc), \end{aligned} \quad (13)$$

and neutral channel polynomials

$$\begin{aligned} \mathcal{B}_{N1}(s_3) &= 2C_x(s_3)\left[\sum_{i=0}^2 H_i X_3^i + H_3 \frac{4Q_3^2}{3s_3} q_{+-}^2(s_3)\right], \\ \mathcal{B}_{N2}(s_3) &= C_{00}(s_3)\left[\sum_{i=0}^2 G_i X_3^i + G_3 \frac{4Q_3^2}{3s_3} q_{00}^2(s_3)\right], \end{aligned} \quad (14)$$

and charged channel polynomials

$$\begin{aligned} \mathcal{B}_{C1}(s_3) &= 2C_{+-}(s_3)\left[\sum_{i=0}^2 H_i X_3^i + H_3 \frac{4Q_3^2}{3s_3} q_{+-}^2(s_3)\right], \\ \mathcal{B}_{C2}(s_3) &= C_x(s_3)\left[\sum_{i=0}^2 G_i X_3^i + G_3 \frac{4Q_3^2}{3s_3} q_{00}^2(s_3)\right], \end{aligned} \quad (15)$$

where

$$\begin{aligned} C_{bc}(s_a) &= C_{bc} + 4D_{bc}q_{bc}^2(s_a) + 16F_{bc}q_{bc}^4(s_a), \\ Q_a^2 &= \frac{\lambda(M_{\eta'}^2, M_a^2, s_a)}{4M_{\eta'}^2}. \end{aligned} \quad (16)$$

The parameters C_i , D_i and F_i are coupling coefficients of $\pi\pi$ interaction and are evaluated by matching to the effective range expansion of $\pi\pi$ scattering, where i represent different

$\pi\pi$ rescattering channels: $(00)\pi^0\pi^0 \rightarrow \pi^0\pi^0; (x)\pi^+\pi^- \rightarrow \pi^0\pi^0; (+-)\pi^+\pi^- \rightarrow \pi^+\pi^-$,

$$\begin{aligned}
C_{00} &= \frac{16\pi}{3}(a_0 + 2a_2)(1 - \xi), \\
C_x &= \frac{16\pi}{3}(a_2 - a_0)\left(1 + \frac{\xi}{3}\right), \\
D_{+-} &= \frac{8\pi}{3}(2a_0 + a_2)(1 + \xi), \\
\xi &= \frac{M_{\pi^\pm}^2 - M_{\pi^0}^2}{M_{\pi^\pm}^2}, \\
D_{00} &= \frac{4\pi}{3}(b_0 + 2b_2), \\
D_x &= \frac{4\pi}{3}(b_2 - b_0), \\
D_{+-} &= \frac{2\pi}{3}(2b_0 + b_2), \\
F_{00} &= \frac{\pi}{3}(f_0 + 2f_2), \\
F_x &= \frac{\pi}{3}(f_2 - f_0), \\
F_{+-} &= \frac{\pi}{6}(2f_0 + f_2),
\end{aligned} \tag{17}$$

where a_i , b_i and f_i are S-wave scattering length, effective ranges and shape parameters of isospin 0 and 2, respectively. a_0 and a_2 are taken as free or fixed parameters in different cases in our study, and b_i are fixed to theoretical value $b_0 = (0.276 \pm 0.006) \times M_\pi^{-2}$, $b_2 = (-0.0803 \pm 0.0012) \times M_\pi^{-2}$, and f_i are fixed to 0. The $\pi\eta$ scattering terms are ignored because the $\pi\eta$ scattering is much weaker than the $\pi\pi$ scattering.

[1] U.-G. Meissner, G. Muller, and S. Steininger, *Phys. Lett. B* **406**, 154 (1997), [Erratum: *Phys.Lett.B* 407, 454 (1997)].
[2] N. Cabibbo, *Phys. Rev. Lett.* **93**, 121801 (2004).
[3] N. Cabibbo and G. Isidori, *JHEP* **03** (2005), 021.
[4] G. Colangelo, J. Gasser, B. Kubis, and A. Rusetsky, *Phys. Lett. B* **638**, 187 (2006).
[5] E. Gamiz, J. Prades, and I. Scimemi, *Eur. Phys. J. C* **50**, 405 (2007).
[6] M. Bissegger, A. Fuhrer, J. Gasser, B. Kubis, and A. Rusetsky, *Nucl. Phys. B* **806**, 178 (2009).

[7] P. Budini and L. Fonda, *Phys. Rev. Lett.* **6**, 419 (1961).
[8] J. R. Batley *et al.* (NA48/2 Collaboration), *Phys. Lett. B* **633**, 173 (2006).
[9] J. R. Batley *et al.* (NA48/2 Collaboration), *Eur. Phys. J. C* **64**, 589 (2009).
[10] M. Bissegger, A. Fuhrer, J. Gasser, B. Kubis, and A. Rusetsky, *Phys. Lett. B* **659**, 576 (2008).
[11] C. Ditsche, B. Kubis, and U.-G. Meissner, *Eur. Phys. J. C* **60**, 83 (2009).
[12] C. O. Gullstrom, A. Kupsc, and A. Rusetsky, *Phys. Rev. C* **79**, 028201 (2009).
[13] E. Abouzaid *et al.* (KTeV Collaboration), *Phys. Rev. D* **78**, 032009 (2008).
[14] C. Adolph *et al.* (WASA-at-COSY Collaboration), *Phys. Lett. B* **677**, 24 (2009).
[15] M. Unverzagt *et al.* (Crystal Ball at MAMI, TAPS, A2 Collaborations), *Eur. Phys. J. A* **39**, 169 (2009).
[16] S. Prakhov *et al.* (Crystal Ball at MAMI, A2 Collaborations), *Phys. Rev. C* **79**, 035204 (2009).
[17] S. Prakhov *et al.* (A2 Collaboration), *Phys. Rev. C* **97**, 065203 (2018).
[18] B. Kubis and S. P. Schneider, *Eur. Phys. J. C* **62**, 511 (2009).
[19] M. Ablikim *et al.* (BESIII Collaboration), *Phys. Rev. D* **97**, 012003 (2018).
[20] P. Adlarson *et al.* (A2 Collaboration), *Phys. Rev. D* **98**, 012001 (2018).
[21] S. Gonzalez-Solıs and E. Passemar, *Eur. Phys. J. C* **78**, 758 (2018).
[22] M. Ablikim *et al.* (BESIII), *Chin. Phys. C* **46**, 074001 (2022).
[23] M. Ablikim *et al.* (BESIII Collaboration), *Nucl. Instrum. Meth. A* **614**, 345 (2010).
[24] M. Ablikim *et al.* (BESIII Collaboration), *Chin. Phys. C* **44**, 040001 (2020).
[25] C. Yu *et al.*, in *7th International Particle Accelerator Conference* (2016) p. TUYA01.
[26] X. Li *et al.*, *Radiat. Detect. Technol. Methods* **1**, 13 (2017).
[27] Y. X. Guo *et al.*, *Radiat. Detect. Technol. Methods* **1**, 15 (2017).
[28] P. Cao *et al.*, *Nucl. Instrum. Meth. A* **953**, 163053 (2020).
[29] J. C. Chen, G. S. Huang, X. R. Qi, D. H. Zhang, and Y. S. Zhu, *Phys. Rev. D* **62**, 034003 (2000).
[30] R. L. Yang, R. G. Ping, and H. Chen, *Chin. Phys. Lett.* **31**, 061301 (2014).
[31] See supplemental material at [URL will be inserted by publisher] for additional information.
[32] S. S. Fang, B. Kubis, and A. Kupsc, *Prog. Part. Nucl. Phys.* **120**, 103884 (2021).
[33] A. E. Bondar *et al.* (Charm-Tau Factory Collaboration), *Phys. Atom. Nucl.* **76**, 1072 (2013).
[34] H. P. Peng, Y. H. Zheng, and X. R. Zhou, *Physics* **49**, 513 (2020).